

TAO, Vol. 17, No. 2, 429-446, June 2006

Doppler Velocity Signatures of Idealized Elliptical Vortices

Wen-Chau Lee^{1, 2, *}, Paul R. Harasti³, Michael Bell², Ben Jong-Dao Jou⁴, and Mou-Hsiang Chang⁵

(Manuscript received 23 April 2005, in final form 22 February 2006)

ABSTRACT

Doppler radar observations have revealed a class of atmospheric vortices (tropical cyclones, tornadoes, dust devils) that possess elliptical radar reflectivity signatures. One famous example is Typhoon Herb (1996) that maintained its elliptical reflectivity structure over a 40-hour period. Theoretical work and dual-Doppler analyses of observed tropical cyclones have suggested two physical mechanisms that can explain the formation of two types of elliptical vortices observed in nature, namely, the combination of a circular vortex with either a wavenumber two vortex Rossby wave or a deformation field. The characteristics of these two types of elliptical vortices and their corresponding Doppler velocity signatures have not been previously examined.

Idealized elliptical vortices consisting of a Rankine vortex combined with wavenumber two disturbances are constructed and sampled by a hypothetical Doppler radar. The Doppler velocity patterns of all wavenumber two cases shown in this study are visually similar. The characteristics of the two-dimensional flow patterns and the corresponding Doppler velocities produced by an idealized vortex Rossby wave and deformation field are illustrated. The ground-based velocity track display (GBVTD) single Doppler vortex wind retrieval technique was performed on these two types of elliptical vortices. The GBVTD technique can retrieve wavenumber two components in the vortex Rossby wave case outside the RMW but failed to retrieve wavenumber two structure of the deformation case for all radii. It

¹ Earth Observing Laboratory, NCAR, Boulder, USA

² The National Center for Atmospheric Research, Boulder, USA

³ Marine Meteorology Division, Naval Research Laboratory, Monterey, USA

⁴ Department of Atmospheric Science, National Taiwan University, Taipei, Taiwan, ROC

⁵ National Defense University, Taoyuan, Taiwan, ROC

* Corresponding author address: Dr. Wen-Chau Lee, Earth Observing Laboratory, NCAR, Boulder, USA; E-mail: wenchau@ucar.edu

can be seen that when the phase of the wavenumber two V_T is ahead of V_R by $\pi/4$ with same amplitude, GBVTD coefficients A3 and B3 are near zero; hence, GBVTD technique cannot retrieve the wavenumber two amplitude in these conditions. However, by knowing the elliptical shape of the vortex as a priori these two mechanisms can still be distinguished by the characteristics of the corresponding GBVTD coefficients.

[Key words: Doppler winds, Elliptical vortex, Vortex Rossby waves, Deformation wind field, GBVTD(Ground-Based Velocity Track Display)]

1. INTRODUCTION

The mean composite structure of a tropical cyclone's eyewall is circular with a wavenumber one asymmetry on the right front side of a tropical cyclone (TC) primarily due to storm motion (Shea and Gray 1973; Gray and Shea 1973). Multiple observations from radar and satellite in recent years indicate that non-circular eyewalls (or polygonal eyewalls) are quite common in nature (e.g., Lewis and Hawkins 1982; Muramatsu 1986; Kuo et al. 1999) contrary to earlier beliefs.

Polygonal (non-circular) eyewall radar reflectivity signatures in TCs have been observed by airborne radar (e.g., APS-20E) as early as 1960 in Hurricane Donna (Jordan and Schatzle 1961). Other shapes ranging from ellipses to hexagons have been observed by airborne and land-based radar (e.g., Lewis and Hawkins 1982; Muramatsu 1986; Kuo et al. 1999; Kossin and Schubert 2001). Lewis and Hawkins (1982) attributed the straight edges in the inner eyewall to the partial reflection of inward propagating gravity waves with different wavenumbers and periods (e.g., Kurihara 1976; Willoughby 1978) and concluded that proximity to land is not a requirement for the generation of polygonal TCs. Muramatsu (1986) documented the counter-clockwise rotation of polygonal eyewalls and their periods in Typhoon Wynne (1980). He linked polygonal eyewalls to the multiple vortices within a tornado meso-cyclone (Fujita et al. 1972; Agee et al. 1976) and related the formation of polygonal eyewalls to inertial instability and barotropic instability due to the large azimuthal velocity shear near the eyewall. Muramatsu (1986) also found that the rotation period of these polygons (between 40 to 50 minutes) decreases as the number of corners on the polygon (wavenumber) increases.

Elliptical TCs have drawn particular attention because of the tremendous damage caused by Typhoon Herb (1996) in Taiwan, including the complete destruction of a WSR-88D (RCWF) in northern Taiwan one month after it was installed. In a few observed TC cases, the elliptical shaped reflectivity pattern remains stable for more than several hours (e.g., Kuo et al. 1999; Chang 2000; Reasor et al. 2000; Yamauchi et al. 2002). Mobile Doppler radars have also observed elliptical shaped tornadoes (e.g., Bluestein et al. 2003a, b).

Dual-Doppler radar analyses of elliptical TCs have revealed two types of physical mechanisms. In Hurricane Olivia (1994), Reasor et al. (2000) used airborne Doppler radar data and found the elliptical eyewall consisted of a wavenumber two asymmetry exhibiting two pairs of counter rotating vortices. Both of the elliptical eyewalls in Hurricane Olivia and

Typhoon Herb rotated counterclockwise with periods consistent with vortex Rossby wave (VRW) theory. Yamauchi et al. (2002) used ground-based Doppler radar data to document a type of elliptical eyewall that remained nearly stationary, unlike the rotating cases of Olivia and Herb. A similar near-stationary elliptical reflectivity pattern has been observed in a tornado (Bluestein et al. 2003a, b; Tanamachi et al. 2006). Yamauchi et al. (2002) hypothesized that this flow pattern can be generated by superimposing a deformation field on an axisymmetric vortex. This theory was adopted by Bluestein (2003a, b) to explain an elliptical tornado.

While VRW features have been numerically simulated in TCs (e.g., Wang 2002a, b; Chen and Yau 2001), observational evidence of the existence of VRW is limited. Typhoon Herb (1996), observed by RCWF radar, exhibited by far the most dramatic elliptical eyewall ever documented (Kuo et al. 1999; Chang 2000). Two complete rotations of Herb's elliptical eye, with a period of 144 minutes, were observed at six-minute intervals. Kuo et al. (1999) argued that the elliptic eye in Herb could be explained by a wavenumber two VRW asymmetry superimposed on a circular vortex. The upstream (clockwise) propagation of this wavenumber two asymmetry along the circular vortex corresponds to a downstream (counterclockwise), cyclonic elliptical eye rotation slower than the mean azimuthal velocity. Using the characteristic size, shape, and intensity of Herb, they also confirmed that the 144-minute rotation period in Herb is consistent with the periods computed from the linear theory of a vorticity edge wave on a Rankine vortex (Lamb 1932, p. 231) and the nonlinear theory of the Kirchhoff elliptical vortex (Lamb 1932, p. 232).

Reasor et al. (2000) pointed out that to resolve the vortex Rossby wave with a period of ~ 50 minutes requires datasets with a time resolution of ~ 10 minutes, so their results derived from the airborne Doppler radar data with ~ 30 minute time resolution were inconclusive. Hence, ground-based Doppler radar data (~ 6 minute interval) may be the only viable resource to resolve vortex Rossby waves in the foreseeable future. The fact that elliptical-shaped TCs can be generated by more than one physical mechanism is intriguing from both operational forecast and TC dynamics perspectives. Although the total flow fields of these elliptical-shaped vortices have been examined in numerical models and idealized, analytical simulations, the characteristics of the Doppler velocity patterns of these vortices have not been rigorously examined. From the operational perspective, it is important to know whether the physical mechanisms of these elliptical-shaped vortices can be distinguished from the Doppler velocity patterns.

The Doppler velocity pattern of a Rankine vortex with a wavenumber two tangential wind asymmetry has been simulated in Lee et al. (1999). This idealized vortex possesses a circular streamline with an elliptical isotach rather than the elliptical streamline those authors originally intended to simulate. It has been shown that the ground-based Velocity Track Display (GBVTD, Lee et al. 1999) technique can retrieve both the Rankine vortex and the wavenumber 2 asymmetric tangential wind structures quite accurately. It is important to examine how GBVTD retrieves circulation for these two elliptical vortices.

Section 2 illustrates the processes used to construct elliptical vortices and their corresponding Doppler velocity patterns. The circulations retrieved from the GBVTD technique on these idealized vortices are presented in Section 3. Section 4 presents a discussion on issues relating to these idealized vortices. Conclusions are presented in Section 5.

2. CONSTRUCTING IDEALIZED ELLIPTICAL VORTICES

The basic Rankine vortex centered at $(x, y) = (0, 60)$ km and its Doppler velocity sampled by a hypothetical Doppler radar located at the origin $(x, y) = (0, 0)$ km are illustrated in Fig. 1. This Rankine vortex is constructed the same way as illustrated in Lee et al. (1999) where the radius of maximum wind (RMW) is 20 km and the maximum tangential wind is 50 m s^{-1} , but without any transverse circulation (i.e., no axisymmetric radial wind) for simplicity. In this section, we will illustrate that elliptical vortices can be constructed by superimposing a wavenumber two VRW or a deformation field, and compare these cases with the wavenumber two tangential anomaly only as demonstrated in Lee et al. (1999). Note that this study only simulates the streamlines of these elliptical vortices; therefore, it is assumed an elliptical streamline possesses an elliptical reflectivity structure (i.e., an elliptical vortex).

2.1 Wavenumber Two Tangential Wind Only

A circular vortex with elliptically-shaped isotachs can be constructed by superimposing a wavenumber two tangential disturbance onto a Rankine combined vortex as demonstrated in Lee et al. (1999). In their example, the amplitude of the tangential wind perturbation was 10 m s^{-1} without radial wind perturbation (Fig. 2a), resulting in a vanishing perturbation along the diagonals. The total flow field is presented in Fig. 2b. The orientation of the elliptical isotach is north-south inside the RMW, and east-west outside the RMW. Note that the streamlines are *circular* (not *elliptical*) in their example. The Doppler velocity signature of this flow pattern is illustrated in Fig. 2c. Although this flow field is unrealistic in many aspects, mainly due to the lack of an accompanying perturbation radial wind, it serves as a baseline pattern to compare with the more realistic flow models presented in the following two scenarios.

2.2 Wavenumber Two VRW

It has been shown that vorticity waves (so-called VRW, Montgomery and Kallenbach 1997) live and propagate along vorticity gradients in the inner core of a TC. Their associated potential vorticity mixing processes have been widely accepted as the mechanism to form polygonal eyewall, meso-vortices, and spiral rainbands (e.g., Guinn and Schubert 1993; Montgomery and Kallenbach 1997; Schubert et al. 1999; Kossin et al. 2000). The existence of the VRW in hurricane-like vortices has been simulated in numerical models of varying complexity, ranging from a barotropic, non-divergent, three-region vortex model (e.g., Terwey and Montgomery 2002) to full physics, non-hydrostatic models (e.g., Wang 2002a, b; Chen and Yau 2001). The numerical modeling work of Reasor et al. (2004) presents a new paradigm that VRWs are created to counter-act the tilting of TCs by vertical shear flow; vertical shear acts as a VRW generator when it interacts with a TC, while the VRWs maintain the TC in near-vertical alignment.

As illustrated in Lamb (1932, p 231), the simplest case of an elliptical streamline can be constructed by superimposing a small amplitude (ε , $\varepsilon \ll \text{RMW}$) wavenumber two disturbance on a Rankine vortex with $\text{RMW} = R_{\max}$, center at the origin, and uniform vorticity ζ

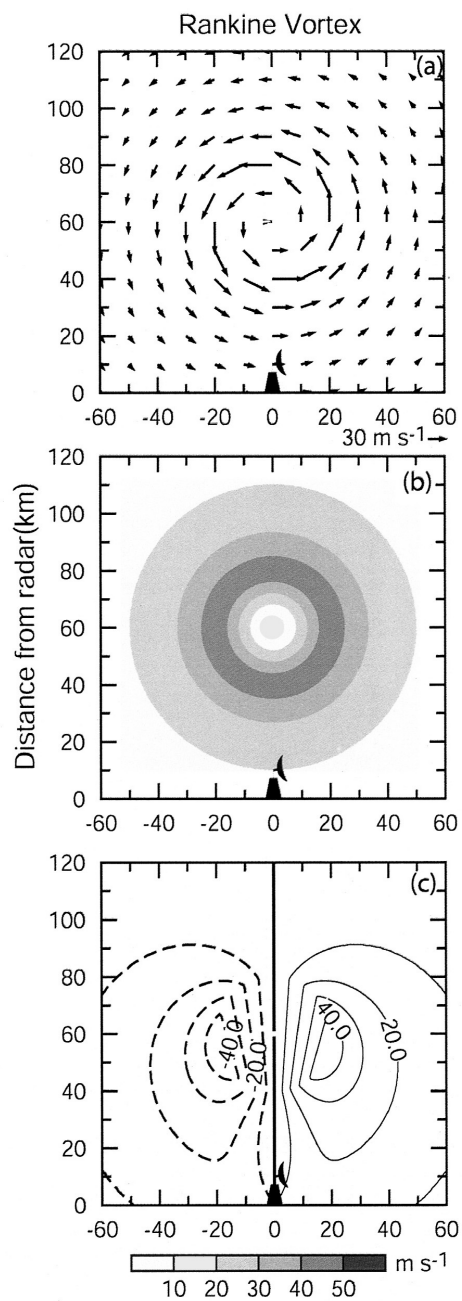


Fig. 1. The basic axisymmetric Rankine combined vortex used in this study: (a) the vector field, (b) the isotach, and (c) the Doppler velocity pattern sampled by a Doppler radar located 60 km south of the vortex center.

inside $R = R_{max}$ as follows:

$$\psi = -\frac{1}{4} \zeta \left[(R_{max}^2 - R^2) - \varepsilon \frac{R^2}{R_{max}} \cos(2\lambda - \omega t) \right] \quad \text{for } R < R_{ell}, \quad (1)$$

$$\psi = -\frac{1}{4} \zeta \left[2R_{max}^2 \ln \frac{R_{max}}{R} - \varepsilon \frac{R_{max}^3}{R^2} \cos(2\lambda - \omega t) \right] \quad \text{for } R > R_{ell}, \quad (2)$$

where $\omega = \zeta/2$ is angular frequency of rotation of the ellipse, λ is the azimuth, R is the radius, and $R_{ell} = R_{max} + \varepsilon \cos(2\lambda - \omega t)$ is the elliptical boundary of maximum winds, not R_{max} .

Equations (1) - (2) represent the general form of the streamfunction for a small-amplitude wavenumber two disturbance located at the edge of a discrete patch of uniform mean vorticity at $R = R_{max}$. In this simple analytic case, the mean vorticity gradient is zero everywhere except at R_{max} , supporting stable wave perturbations, which rotate indefinitely. While this may seem to be an extreme idealization, numerical simulations of the quasi-steady rotation of Typhoon Herb's elliptical eye suggest that this simple linear wave model can produce surprisingly similar behavior (Kuo et al. 1999). It is a straight forward matter to derive the azimuthal and radial velocities of this system from (1) and (2) as follows:

$$V_T = \frac{\partial \psi}{\partial R} = \frac{1}{2} \zeta R \left[1 + \frac{\varepsilon}{R_{max}} \cos(2\lambda - \omega t) \right] \quad \text{for } R < R_{ell}, \quad (3)$$

$$V_T = \frac{\partial \psi}{\partial R} = \frac{1}{2} \zeta \frac{R_{max}^2}{R} \left[1 - \varepsilon \frac{R_{max}}{R^2} \cos(2\lambda - \omega t) \right] \quad \text{for } R > R_{ell}, \quad (4)$$

$$V_R = -\frac{1}{R} \frac{\partial \psi}{\partial \lambda} = \frac{1}{2} \zeta R \left[\frac{\varepsilon}{R_{max}} \sin(2\lambda - \omega t) \right] \quad \text{for } R < R_{ell}, \quad (5)$$

$$V_R = -\frac{1}{R} \frac{\partial \psi}{\partial \lambda} = \frac{1}{2} \zeta \frac{R_{max}^2}{R} \left[\varepsilon \frac{R_{max}}{R^2} \sin(2\lambda - \omega t) \right] \quad \text{for } R > R_{ell}. \quad (6)$$

The magnitude of the tangential and radial velocities of the idealized wavenumber two disturbance is the same while their phase difference is $\pi/4$ at all radii. The radial wind wavenumber two disturbance is continuous across R_{ell} , while the tangential wavenumber two disturbance is only continuous across R_{ell} to first order of ε in the Taylor series expansion of R_{ell} . As a result, the wavenumber two disturbance manifests itself as two pairs of counter-rotating vortices (Fig. 3a). If one superimposes this disturbance with the Rankine vortex then the resulting

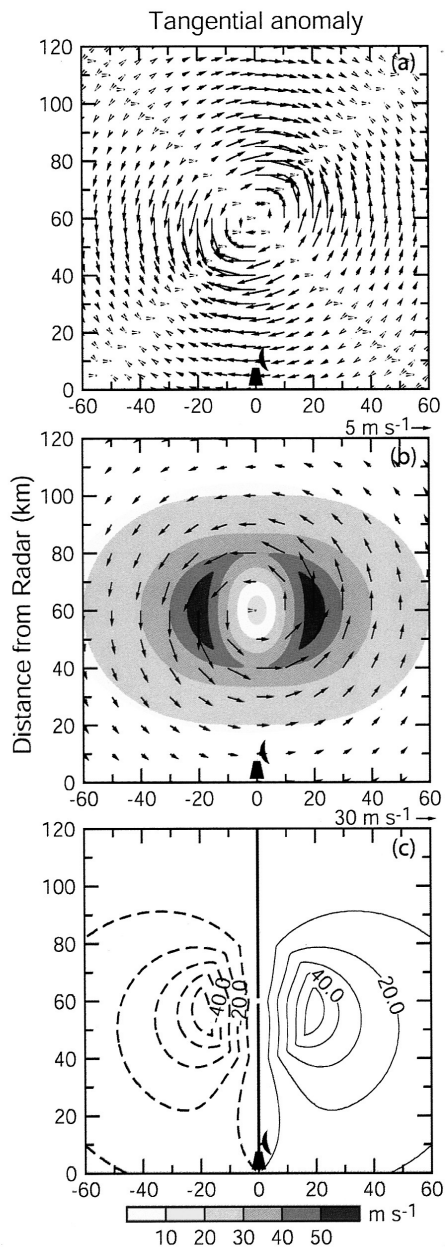


Fig. 2. Elliptical circulation constructed from wavenumber two tangential wind only and a Rankine combined vortex: (a) the perturbation wind field of a wavenumber two tangential wind only, (b) the isotach and vector field of the elliptical vortex, (c) the Doppler velocity pattern of this elliptical vortex.

total circulation is an ellipse. Figure 3b shows the elliptical circulation for the case of a small-amplitude disturbance defined by $\varepsilon = 3$ km, with an amplitude of 7.1 m s^{-1} . Note that the total wind speed is a constant along an ellipse and the orientation of the ellipse remains east-west for all radii. The corresponding Doppler velocity pattern is shown in Fig. 3c, where only subtle differences can be identified compared with Figs. 1c and 2c.

2.3 Deformation Field

A pure deformation field can be constructed as follows (e.g., Bluestein 1993):

$$u = D/2[x \cos(2\gamma) + y \sin(2\gamma)] , \quad (7)$$

$$v = D/2[x \sin(2\gamma) - y \cos(2\gamma)] , \quad (8)$$

where D is the magnitude of the deformation (0.2 s^{-1} in this example), γ is the angle of the axis of dilation (45° in this example), x and y are the distance to the center (stagnation point) of the deformation field. A pure deformation field is neither rotational nor divergent (Bluestein 1993, p. 99), and the magnitude of the velocity increases linearly with the radius (distance between a point and the stagnation point).

The deformation field is illustrated in Fig. 4a and the total elliptical flow field by superimposing the deformation field to the Rankine vortex is illustrated in Fig. 4b. The elliptical isolachs shown in Figs. 2b and 4b are very similar because their corresponding asymmetric component shown in Figs. 2a and 4a are qualitatively similar. Thus, the wavenumber two tangential wind anomaly only case (Lee et al. 1999) captures half of the deformation field characteristics illustrated here. Accordingly, the Doppler velocity pattern of the deformation field (Fig. 4c) is quite similar to the wavenumber two tangential wind only case (Fig. 2c). It should be noted, however, that the streamlines shown in Fig. 2b are circular whereas the streamlines shown in Fig. 4b are elliptical. An interesting feature is that the major axis of the elliptical streamlines in Fig. 4b is perpendicular to the major axis of the elliptical isolachs.

The similarities between the wavenumber two tangential wind only case and the deformation field case can be illustrated as follows. Representing V_T and V_R in terms of Cartesian u and v , it can be shown that the deformation field possesses a wavenumber two characteristics in cylindrical coordinates as follows:

$$V_T = v \cos \lambda - u \sin \lambda , \quad (9)$$

$$V_R = u \cos \lambda + v \sin \lambda , \quad (10)$$

where λ is the azimuth of the cylindrical coordinates. Using the relations $x = R \cos \lambda$ and $y = R \sin \lambda$ in (7) and (8), then substituting the results into (9) and (10) while utilizing the trigonometric identities $\sin 2\phi = 2 \sin \phi \cos \phi$ and $\cos 2\phi = \cos^2 \phi - \sin^2 \phi$, we obtain:

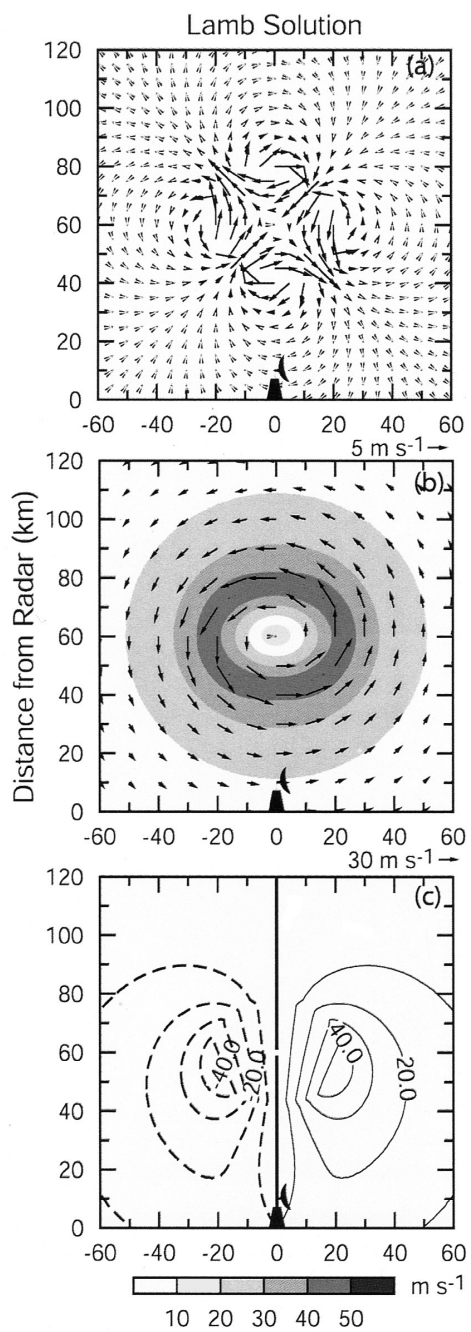


Fig. 3. Same as Fig. 2 but for the elliptical vortex constructed by a wavenumber two vortex Rossby wave and a Rankine combined vortex.

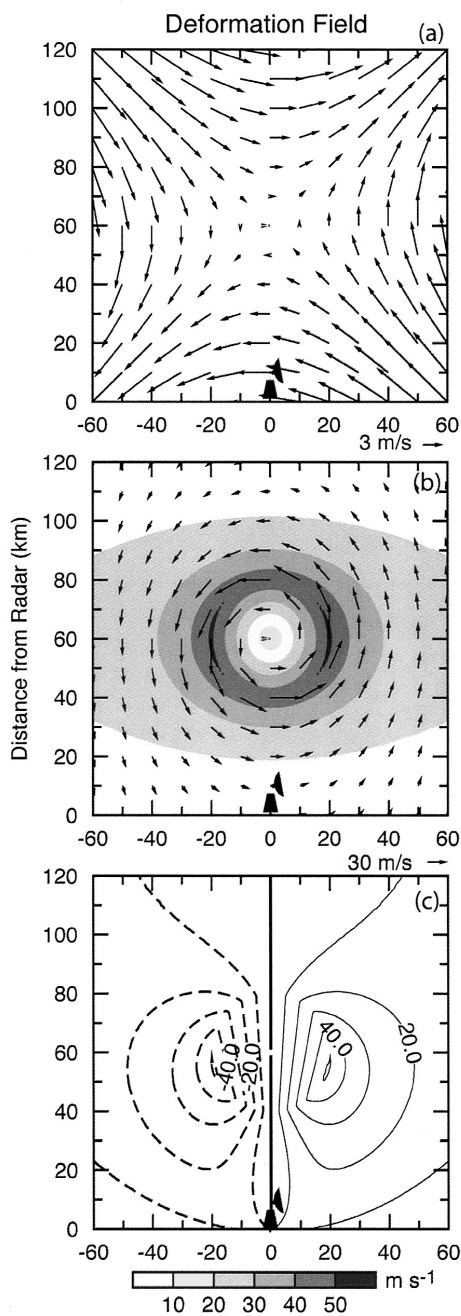


Fig. 4. Same as Fig. 2 but for the elliptical vortex constructed by a modified deformation field and a Rankine combined vortex.

$$V_T = \frac{DR}{2} [-\sin 2\lambda \cos 2\gamma + \cos 2\lambda \sin 2\gamma] = -\frac{DR}{2} \sin 2(\lambda - \gamma) , \quad (11)$$

$$V_R = \frac{DR}{2} [\cos 2\lambda \cos 2\gamma + \sin 2\lambda \sin 2\gamma] = \frac{DR}{2} \cos 2(\lambda - \gamma) . \quad (12)$$

Hence, the V_T and V_R signatures of a deformation field are wavenumber two and are continuous for all radii. Note that the phase relationship in the deformation field between V_T in (11) and V_R in (12) is analogous to the VRW phase relationship inside the RMW in (3) and (5). In both cases, the phase of V_T lags behind V_R by 45° .

3. GBVTD ANALYSIS

In Section 2, three vortices with elliptical characteristics constructed with different perturbation flow fields were shown to possess very similar Doppler velocity signatures. Visually, it is unlikely that even an experienced researcher/forecaster could distinguish the subtle differences among these seemingly identical Doppler velocity patterns. However, these differences in the Doppler velocities contain critical information about vortex kinematics and dynamics.

Equations (24) and (25) in Lee et al. (1999) state that:

$$\begin{aligned} V_T S_2 + V_R C_2 &= 2A3 , \\ V_T C_2 - V_R S_2 &= -2B3 , \end{aligned} \quad (13)$$

where A3 and B3 are the wavenumber three GBVTD Fourier coefficients (corresponding to wavenumber two of the vortex circulation), and $V_T S_2$ ($V_R S_2$) and $V_T C_2$ ($V_R C_2$) are the sine and cosine wavenumber two components of the tangential (radial) wind, respectively. Thus, there are two equations with four unknowns requiring additional closure assumptions in order to solve for the wind field. The closure assumptions for GBVTD were:

$$V_R C_2 = V_R S_2 = 0 . \quad (14)$$

In this section, we will examine characteristics of the GBVTD analyses on these idealized vortices based on the aforementioned closure assumptions.

3.1 Tangential Wavenumber Two Only

The GBVTD-retrieved isotachs of the tangential wavenumber two only case are illustrated in Fig. 5a. Since this situation exactly matched the GBVTD assumption, it is not surprising that the wavenumber two tangential wind anomalies are almost completely retrieved with some distortion in the retrieved wind field compared with the original isotach in Fig. 2b. The

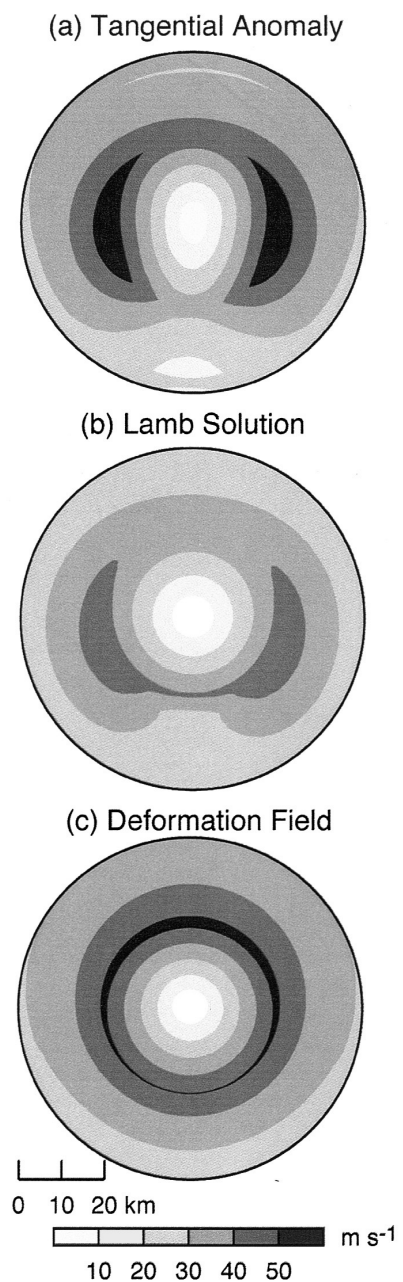


Fig. 5. GBVTD retrieved isotach from the elliptical vortices constructed by a wavenumber two disturbance from: (a) tangential anomaly only, (b) the vortex Rossby wave (Lamb solution), and (c) the deformation field.

geometric distortion in the GBVTD retrieved isotachs has been illustrated in Lee et al. (1999). This case is provided here for comparison purposes.

3.2 Wavenumber Two VRW

The GBVTD retrieved isotachs of the wavenumber two VRW are illustrated in Fig. 5b. Compared with the isotachs in Fig. 3b, it is clear that the GBVTD technique can retrieve the elliptical isotach oriented in the east-west direction as shown in Fig. 3b. However, the wind maxima along the minor axis (north-south direction) could not be retrieved. Although the GBVTD technique can identify a wavenumber two structure, the two counter-rotating vortices in the original wavenumber two disturbances are not retrieved with only the tangential wind anomaly in the GBVTD formulation.

A more detailed look of the decomposition on each wavenumber is illustrated in Fig. 6. The GBVTD-retrieved mean tangential wind (wavenumber zero) is weaker than the original Rankine vortex where a 10 m s^{-1} (20%) discrepancy occurred at the R_{\max} . A false wavenumber one is retrieved (Fig. 6a) where there is no wavenumber one in the original vortex. The original and retrieved wavenumber two components are shown in Fig. 6b. The GBVTD retrieved wavenumber two V_T is larger than the original V_T outside R_{\max} due to the aliasing of V_R into V_T . The retrieved wavenumber two V_T inside R_{\max} is near zero and there is a transition zone near R_{\max} . Nevertheless, the GBVTD technique is able to recognize a wavenumber two signature from the single Doppler velocity pattern.

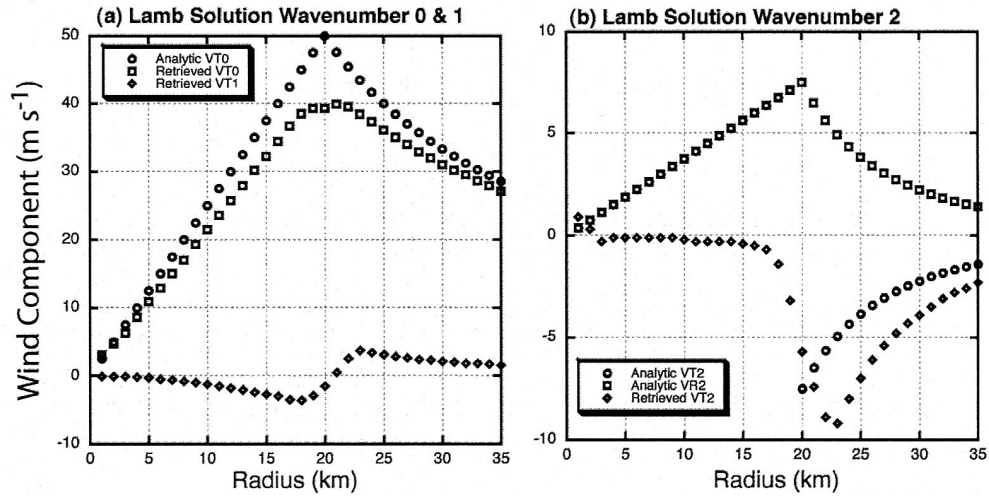


Fig. 6. Comparisons between the input and GBVTD-retrieved amplitudes on a vortex Rossby wave wavenumber two disturbance: (a) wavenumber zero and one, and (b) wavenumber two.

3.3 Deformation Field Case

The retrieved total wind (isotachs shown in Fig. 5c) does not resemble the original elliptical flow pattern (Fig. 4b), but is instead similar to a Rankine vortex plus a small wavenumber one asymmetry (Fig. 12a in Lee et al. 1999). The parent Rankine vortex is nearly retrieved completely (overestimate by 1 - 2 m s⁻¹ on the peak tangential wind) while the deformation field is incorrectly represented by a small wavenumber one and a smaller wavenumber two disturbance (Fig. 7), possibly due again to spectral leakage. The amplitude of the false wavenumber one is twice the amplitude of the false wavenumber two but both of them are so small that they can be ignored for practical purposes. This signature is similar to that appearing in the inner region (inside R_{max}) of the VRW wavenumber two results illustrated in Fig. 6b. We have shown that the phase relationships between V_T and V_R are identical everywhere in the domain. This again shows that the GBVTD technique has limitations in retrieving asymmetric circulations when the phase of the asymmetric V_T leads V_R by $\pi/4$ in a wavenumber two disturbance.

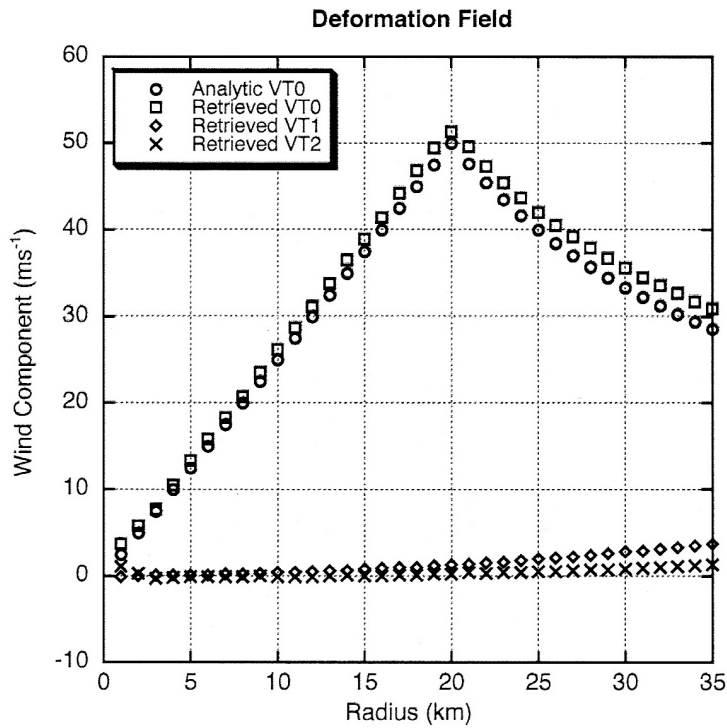


Fig. 7. Comparisons between the input and GBVTD-retrieved amplitudes on wavenumber zero, one and two for the deformation field case. In this case, there is no initial wavenumber one amplitude.

4. DISCUSSION

(a) Both the elliptical vortices constructed from the wavenumber two VRW and the deformation field are physically plausible, which are improvements over the wavenumber two tangential anomaly only flow field proposed in Lee et al. (1999). This study demonstrates that the Doppler velocity patterns of the parent Rankine vortex and these three distinct wavenumber two flow fields are quite similar with very subtle differences (Figs. 1c, 2c, 3c, and 4c). Although the GBVTD analyses on three similar Doppler velocity patterns cannot retrieve the complete flow structures in the two new elliptical vortices introduced in this study, the GBVTD coefficients do show distinct signatures for all three types of wavenumber two vortices. By knowing the elliptical shape of the vortex as a priori, the characteristics of the GBVTD coefficients can be used to distinguish wavenumber two structures/mechanisms between deformation and VRW, if one assumes these physical mechanisms are responsible for the elliptical flow.

(b) Although the results are encouraging, this study rules out the possibility that the quasi-steady elliptical shaped tornado observed by Bluestein et al. (2003b) was generated by a deformation field because their GBVTD analysis did resolve significant wavenumber two components which would not have been resolved if deformation was the underlying process. Their study also ruled out the possibility of aliasing due to tornado evolution during the fast scan time of ~ 6 s by their W-band mobile radar. However, it is possible that aliasing could occur in a fast moving and a small RMW (~ 80 m) tornado because of the vortex being considered stationary over the duration of the scan (Tanamachi et al. 2006). It is also possible that another physical mechanism beyond those proposed in this study is responsible for the case study documented in Bluestein et al. (2003b). For example, quasi, non-rotating, elliptical circulations have also been revealed in both observational and modeling studies; however, unlike the elliptical circulations considered in this study, the circulation center was not located at the geometric center of the ellipse (e.g., Moss and Jones 1978; Brandes 1984; Bluestein and Hazen 1989; Desrochers and Harris 1996). The authors are also aware of a similar situation documented in Shapiro (1983) where a numerically simulated TC possessed a wavenumber two structure in the boundary layer produced by the interactions between the TC circulation and surface friction effects. Due to the near-surface scanning strategy utilized in Bluestein et al. (2003b), it is possible that frictional effects could play a strong role in determining the asymmetry of the circulation at that altitude.

(c) As one of the reviewers pointed out, a wavenumber two VRW can sit on top of a deformation field. This situation indeed would complicate the problem. If the synoptic deformation field has the same center as the wavenumber two VRW, the GBVTD analysis would still show a VRW signature since GBVTD cannot resolve the deformation field. However, the reflectivity structure may show a complex structure as the VRW rotated through the near stationary deformation field. If the deformation field is not collocated with the VRW, the current approach would have difficulties interpreting and analyzing the flow field.

(d) Although the authors only show results from one viewing angle (from south of a vortex), examining cases from other viewing angles indicated that the bulk properties hold in general and minor variations in the retrieved amplitudes in each of the terms exist for each of

the three cases shown here owing to the intrinsic geometric distortion in the GBVTD technique (Lee et al. 1999). As a result, the results presented in this paper are representative from all viewing angles by a Doppler radar.

5. SUMMARY

This paper presents an overview of elliptical wind fields constructed by superimposing three different wavenumber two perturbations onto a Rankine vortex, namely: (1) a wavenumber two tangential wind only as illustrated in Lee et al. (1999), (2) a small amplitude wavenumber two VRW, and (3) a deformation field. It is shown that the deformation field possesses a wavenumber two signature in cylindrical coordinates. The characteristics of the total winds, perturbation winds, and corresponding Doppler velocity patterns of these three elliptical vortices are presented. The total winds in all three cases resemble variations of vortices with elliptical characteristics. The similarities in the isotachs, Doppler velocity patterns, and GBVTD signatures between the wavenumber two VRW and the deformation field are intriguing. The challenge inherent in distinguishing these subtle differences in the Doppler velocity patterns has been demonstrated.

The GBVTD analyses only perform well on the wavenumber two tangential anomaly only case. When including wavenumber two asymmetric radial wind components to construct elliptical vortices, GBVTD can only partially deduce the full circulations in the VRW and deformation cases. It can be seen that when the phase of the wavenumber two V_T is ahead of V_R by $\pi/4$ with equal amplitude, GBVTD coefficients A3 and B3 vanish. This situation happens in the deformation case and inside the RMW for the VRW wavenumber two case where only the parent Rankine vortex can be retrieved by the GBVTD technique. Nevertheless, by combining the characteristics of the GBVTD coefficients and a priori knowledge that an elliptical vortex is present, the underlying physical mechanisms of these two types of elliptical vortices can still be inferred from the GBVTD analyses, as long as one of these mechanisms is responsible for the elliptical flow. It appears that another mechanism in addition to those two mechanisms discussed in this study is capable of producing a near stationary (i.e., non-rotating) elliptical vortex possessing wavenumber two GBVTD characteristics as documented in Bluestein et al. (2003b).

Although the GBVTD analyses show encouraging results in deducing these elliptical vortices, it is evident that the GBVTD technique in its current framework has limitations. More complicated closure assumptions other than simply assuming asymmetric $V_R \ll V_T$ are needed in order to improve the retrieval of elliptical vortex circulations. The elliptical vortices presented in this study (i.e., VRW wavenumber two and deformation) provide additional physical constraints to the GBVTD formulation. An improved GBVTD formulation that takes into account the aforementioned constraints will be presented in a future paper.

REFERENCES

- Agee, E. M., J. T. Snow, and P. R. Care, 1976: Multiple vortex feature in the tornado cyclone and the occurrence of tornado families. *Mon. Wea. Rev.*, **104**, 522-563.

- Bluestein, H. B., and D. S. Hazen, 1989: Doppler-radar Analysis of a tropical cyclone over land: Hurricane Alicia (1983) in Oklahoma. *Mon. Wea. Rev.*, **117**, 2594-2611.
- Bluestein, H. B., 1993: Synoptic-Dynamic Meteorology in Midlatitudes. Volume I: Principles of Kinematics and Dynamics. Oxford, 431 pp.
- Bluestein, H. B., C. Weiss, and A. L. Pazmany, 2003a: Mobile Doppler radar observations of a tornado in a supercell near Bassett, Nebraska, on 5 June 1999. Part I: Tornadogenesis. *Mon. Wea. Rev.*, **131**, 2954-2967.
- Bluestein, H. B., W. C. Lee, M. Bell, C. Weiss, and A. L. Pazmany, 2003b: Mobile Doppler radar observations of a tornado in a supercell near Bassett, Nebraska, on 5 June 1999. Part II: Tornado vortex structure. *Mon. Wea. Rev.*, **131**, 2955-2984.
- Brandes, E. A., 1984: Vertical vorticity generation and mesocyclone sustenance in tornadic thunderstorms: The observational evidence. *Mon. Wea. Rev.*, **112**, 2253-2269.
- Chang, P. L., 2000: Circulation Change Analysis on landfalling Typhoon: A case study Herb (1996). Ph.D. dissertation, Nat. Taiwan Univ., Taipei, Taiwan, 158 pp.
- Chen, Y., and M. K. Yau, 2001: Spiral bands in a simulated hurricane. Part I: Vortex Rossby wave verification. *J. Atmos. Sci.*, **58**, 2128-2145.
- Desrochers, P. R., and F. I. Harris, 1996: Interpretation of mesocyclone vorticity and divergence structure from single-Doppler radar. *J. Appl. Meteor.*, **35**, 2191-2209.
- Fujita, T. T., K. Watanabe, K. Tsuchiya, and M. Shimada, 1972: Typhoon-associated tornadoes in Japan and new evidence of suction vortices in a tornado near Tokyo. *J. Meteor. Soc. Japan*, **50**, 431-453.
- Gray, W. M., and D. J. Shea, 1973: The hurricane's inner core region. Part II: Thermo-stability and dynamic characteristics. *J. Atmos. Sci.*, **30**, 1565-1576.
- Guinn, T. A., and W. H. Schubert, 1993: Hurricane spiral bands. *J. Atmos. Sci.*, **50**, 3380-3403.
- Jordan, C. L., and F. J. Schatzle, 1961: The "double eye" of Hurricane Donna. *Mon. Wea. Rev.*, **89**, 354-356.
- Kossin, J. P., and W. Schubert, 2001: Mesovortices, polygonal flow patterns, and rapid pressure falls in hurricane-like vortices. *J. Atmos. Sci.*, **58**, 2196-2209.
- Kossin, J. P., W. H. Schubert, and M. T. Montgomery, 2000: Unstable Interactions between a Hurricane's Primary Eyewall and a Secondary Ring of Enhanced Vorticity. *J. Atmos. Sci.*, **57**, 3893-3917.
- Kuo, H. C., R. T. Williams, and J. H. Chen, 1999: A possible mechanism for the eye rotation of Typhoon Herb. *J. Atmos. Sci.*, **56**, 1659-1673.
- Kurihara, Y., 1976: On the development of spiral bands in a tropical cyclone. *J. Atmos. Sci.*, **33**, 940-958.
- Lamb, H., 1932: Hydrodynamics. 6th ed. Dover, 732 pp.
- Lee, W. C., J. D. Jou, P. L. Chang, and S. M. Deng, 1999: Tropical cyclone kinematic structure retrieved from single Doppler radar observations. Part I: Interpretation of Doppler velocity patterns and the GBVTD technique. *Mon. Wea. Rev.*, **127**, 2419-2439.
- Lewis, B. M., and H. F. Hawkins, 1982: Polygonal eye walls and rainbands in hurricanes. *Bull. Am. Meteor. Soc.*, **63**, 1294-1300.

- Montgomery, M. T., and R. J. Kallenbach, 1997: A theory for vortex Rossby-waves and its application to spiral bands and intensity changes in hurricanes. *Quart. J. Roy. Meteor. Soc.*, **123**, 435-465.
- Moss, M. S., and R. W. Jones, 1978: A numerical simulation of hurricane landfall. NOAA Technical Memorandum ERL NHEML-3, National Hurricane and Experimental Meteor. Lab., Coral Gables, Florida, United States Department of Commerce, 21 pp.
- Muramatsu, I., 1986: The structure of polygonal eye of a typhoon. *J. Meteor. Soc. Japan*, **64**, 913-921.
- Reasor, P. D., M. T. Montgomery, F. D. Marks, Jr., and J. F. Gamache, 2000: Low-wavenumber structure and evolution of the hurricane inner core observed by airborne dual-Doppler radar. *Mon. Wea. Rev.*, **128**, 1653-1680.
- Reasor, P. D., M. T. Montgomery and L. D. Grasso, 2004: A new look at the problem of tropical cyclones in vertical shear flow: Vortex resiliency. *J. Atmos. Sci.*, **61**, 3-22.
- Schubert, W. H., M. T. Montgomery, R. K., Taft, T. A. Guinn, S. R. Fulton, J. P. Kossin, and J. P. Edwards, 1999: Polygonal eyewalls, asymmetric eye contraction, and potential vorticity mixing in hurricanes. *J. Atmos. Sci.*, **56**, 1197-1223.
- Shapiro, L. J., 1983: The asymmetric boundary layer flow under a translating hurricane. *J. Atmos. Sci.*, **40**, 1984-1998.
- Shea, D. J., and W. M. Gray, 1973: The hurricane's inner core region. Part I: Symmetric and asymmetric structure. *J. Atmos. Sci.*, **30**, 1544-1564.
- Tanamachi, R. L., H. B. Bluestein, W. C. Lee, M. Bell, and A. Pazmany, 2006: Ground-based velocity track display (GBVTD) analysis of a W-band Doppler radar data in a tornado near Stockton, Kansas, on 15 May 1999. *Mon. Wea. Rev.*, (Accepted with revision).
- Terwey, W. D., and M. T. Montgomery, 2002: Wavenumber-2 and Wavenumber-m Vortex Rossby Wave Instabilities in a Generalized Three-Region Model. *J. Atmos. Sci.*, **59**, 2421-2427.
- Wang, Y., 2002a: Vortex Rossby waves in a numerically simulated tropical cyclone. Part I: Overall structure, potential vorticity and kinetic energy budgets. *J. Atmos. Sci.*, **59**, 1213-1238.
- Wang, Y., 2002b: Vortex Rossby waves in a numerically simulated tropical cyclone. Part II: The role in tropical cyclone structure and intensity changes. *J. Atmos. Sci.*, **59**, 1239-1262.
- Willoughby, H. E., 1978: A possible mechanism for the formation of hurricane rainbands. *J. Atmos. Sci.*, **35**, 836-848.
- Yamauchi, H., O. Suzuki, and K. Akaeda, 2002: Asymmetry in wind field of Typhoon 0115 analyzed by triple Doppler radar observations. Int. Conf. on Mesoscale Convective Systems and Heavy Rainfall/Snowfall in East Asia. Tokyo, Japan, 245-250.

Lee, W. C., Harasti, P. R., Bell, M., Jou, B. J. D., and Chang, M. H., 2006: Doppler velocity signatures of idealized elliptical vortices. Terr. Atmos. Ocean. Sci., **17**, 429-446.